

The Role of Water Vapor Feedback in Unperturbed Climate Variability and Global Warming

ALEX HALL*

Atmospheric and Oceanic Sciences Program, Princeton University, Princeton, New Jersey

SYUKURO MANABE[†]

Geophysical Fluid Dynamics Laboratory, Princeton, New Jersey

(Manuscript received 6 November 1997, in final form 9 June 1998)

ABSTRACT

To understand the role of water vapor feedback in unperturbed surface temperature variability, a version of the Geophysical Fluid Dynamics Laboratory coupled ocean–atmosphere model is integrated for 1000 yr in two configurations, one with water vapor feedback and one without. For all spatial scales, the model with water vapor feedback has more low-frequency (timescale ≥ 2 yr) surface temperature variability than the one without. Thus water vapor feedback is positive in the context of the model's unperturbed variability. In addition, water vapor feedback is more effective the longer the timescale of the surface temperature anomaly and the larger its spatial scale.

To understand the role of water vapor feedback in global warming, two 500-yr integrations were also performed in which CO₂ was doubled in both model configurations. The final surface global warming in the model with water vapor feedback is 3.38°C, while in the one without it is only 1.05°C. However, the model's water vapor feedback has a larger impact on surface warming in response to a doubling of CO₂ than it does on internally generated, low-frequency, global-mean surface temperature anomalies. Water vapor feedback's strength therefore depends on the type of temperature anomaly it affects. The authors found that the degree to which a surface temperature anomaly penetrates into the troposphere is a critical factor in determining the effectiveness of its associated water vapor feedback. The more the anomaly penetrates, the stronger the feedback. It is also shown that the apparent impact of water vapor feedback is altered by other feedback mechanisms, such as albedo and cloud feedback. The sensitivity of the results to this fact is examined.

Finally, the authors compare the local and global-mean surface temperature time series from both unperturbed variability experiments to the observed record. The experiment without water vapor feedback does not have enough global-scale variability to reproduce the magnitude of the variability in the observed global-mean record, whether or not one removes the warming trend observed over the past century. In contrast, the amount of variability in the experiment with water vapor feedback is comparable to that of the global-mean record, provided the observed warming trend is removed. Thus, the authors are unable to simulate the observed levels of variability without water vapor feedback.

1. Introduction

The precise amount of warming that would take place for a given increase in greenhouse gases in the atmosphere remains an unknown quantity. According to the latest Intergovernmental Panel on Climate Change as-

essment, the likely equilibrium global-mean temperature response to a doubling of CO₂ ranges from 1.5° to 4.5°C (Intergovernmental Panel on Climate Change 1996). The source of this uncertainty is our inability to quantify the role of feedback mechanisms in the climate system, including water vapor, cloud, lapse rate, and albedo feedback. Water vapor feedback, the subject of this study, has long been thought to be a positive feedback mechanism (see, e.g., Manabe and Wetherald 1967). This is due to the dependence of the saturation water vapor mixing ratio on temperature, as predicted by the Clausius–Clapeyron equation. Thus a CO₂-induced warming of the surface–troposphere system will lead to a water vapor increase in the atmosphere. Since water vapor is itself a greenhouse gas, this increase will reduce the longwave radiative damping of the temper-

* Current affiliation: Lamont-Doherty Earth Observatory, Columbia University, Palisades, New York.

[†] Current affiliation: Earth Frontier Research System, Tokyo, Japan.

Corresponding author address: Alex Hall, Lamont-Doherty Earth Observatory of Columbia University, Oceanography Bldg., Room 103, P.O. Box 1000, 61 Route 9W, Palisades, NY 10964-8000.
E-mail: alexhall@rosie.ldeo.columbia.edu

ature anomaly, making the warming larger than it would be otherwise. While there is a consensus that water vapor feedback is positive in the context of global warming, it remains unclear exactly how strong the effect is (Dickinson et al. 1996). Large uncertainties also exist regarding the magnitude (and sign, in the case of cloud feedback) of the other feedback mechanisms.

If a particular feedback mechanism is an important factor in greenhouse-gas-induced climate change, it ought to play an important role in unperturbed variability as well. To take the example of water vapor feedback, suppose an internally generated forcing, such as a change in net cloud cover associated with atmospheric disturbances, were to induce a warm anomaly in the surface–troposphere system. A resulting increase in atmospheric water vapor and hence greenhouse trapping of outgoing radiation would reduce the radiative damping of the anomaly. This, in turn, will increase its magnitude. Similarly, since colder air holds less water vapor, a cold surface–troposphere anomaly ought to be associated with reduced water vapor mixing ratios. This would enhance the outgoing longwave radiation, making the anomaly cooler than if there were no decrease in water vapor. Thus while water vapor feedback plays no role in generating the temperature anomalies themselves, whether externally forced or internally generated, it ought to have a significant impact on their magnitude. In this way, water vapor feedback can be said to “enhance” or “amplify” temperature anomalies of the surface–troposphere system.

Despite its importance to the sensitivity and variability of climate, a comprehensive picture of water vapor feedback’s impact on both externally forced and internally generated climate variations is lacking. For example, it is completely unknown whether water vapor feedback amplifies an externally forced climate fluctuation, such as that arising from an increase in greenhouse gases, to the same degree that it amplifies internally generated climate variations. If this were the case, it would obviously be of enormous importance, because water vapor feedback’s contribution to the sensitivity of the climate to a greenhouse gas increase could be estimated from unperturbed variability alone. In addition, the impact of water vapor feedback on unperturbed temperature variability is itself very poorly characterized: does water vapor feedback’s strength depend on the timescale of an internally generated temperature anomaly? On its spatial scale? Addressing these fundamental issues using a coupled ocean–atmosphere model is the goal of this study. In so doing, we aim to develop a comprehensive, albeit qualitative, picture of the basic operation of water vapor feedback.

These issues have never been directly addressed before because they are impossible to study using the observed record alone. It has only been within the past few years that satellite data measuring water vapor content, outgoing longwave radiation, and surface temperature have become available. Even assuming this dataset

is accurate, it is still too short to give reliable statistics on many aspects of water vapor feedback and is likely to remain so for quite some time. A numerical model of the climate, on the other hand, provides long time series with global coverage that are reliable in a statistical sense. Moreover, a numerical model is a very flexible scientific tool because any physical mechanism it includes may be removed from the simulation and the effect of the mechanism may be diagnosed. In this study, we disable the water vapor feedback of a coupled ocean–atmosphere model by fixing the water vapor mixing ratios to their climatological mean values in the longwave portion of the model’s radiative transfer subroutine. Thus anomalies in water vapor predicted by the model’s hydrological component are not taken into account in the longwave radiative transfer calculation. In this way, if atmospheric water vapor increases due to a warm surface temperature anomaly, for example, that change in water vapor will not result in any increased greenhouse trapping. In this study, we also employ a model configuration where water vapor is allowed to interact with longwave radiation, as the model was originally designed. By comparing the variability that results from unperturbed long-term integrations of the two model configurations with and without water vapor feedback (referred to hereafter as the control and fixed H₂O configurations), we can measure directly the impact of water vapor feedback on the model’s unperturbed variability in a way that is not feasible through analysis of the observed record. Unlike the real world, we can also manipulate at will the concentrations of greenhouse gases in a numerical model. Thus we can measure the warming that results in the control and fixed H₂O configurations when CO₂ is gradually increased and then held fixed at twice its original value. This, in turn, allows us to compare the role of water vapor feedback in greenhouse-gas-induced global warming to its role in unperturbed variability. Since the suppression of unperturbed variability and the reduction of global warming in the fixed H₂O model are attributable to the same physical mechanism, our approach is self-consistent.

The presentation of this study is structured as follows. First, we give a detailed description of the numerical model (section 2) and the experimental technique (section 3) used in these simulations. In section 4, the analysis of water vapor feedback’s role in unperturbed variability is presented. The main focus in this section is the dependence of water vapor feedback’s strength on the time and spatial scale of the temperature anomaly it affects. In section 5, the results of the global warming experiments are given and comparisons are made between the contributions of water vapor feedback to climate sensitivity in the unperturbed variability and global warming contexts. Then, in section 6, we examine the way in which other feedback mechanisms, such as albedo and cloud feedback, alter the apparent impact of water vapor feedback in both the unperturbed variability and global warming contexts. Section 7a outlines the

main conclusions of the analysis. Finally, in section 7b, we place the fixed H₂O and control simulations in the context of the real climate. By comparing the unperturbed temperature variability of the fixed H₂O and control simulations to the observed temperature record, we assess whether the model's water vapor feedback is necessary to simulate the observed levels of variability.

2. Model structure and time integration

The most important features of this model are described in some detail in Manabe et al. (1991). It consists of a general circulation model of the world ocean coupled to an atmospheric general circulation model through exchange of heat, water, and momentum. The model includes those features of the earth's geography that its resolution permits. It also has a seasonal cycle of insolation, although the diurnal cycle is not included.

The variables of the atmospheric component are represented in the horizontal by a series of spherical harmonics and corresponding gridpoint values. Fifteen zonal waves and associated Legendre functions are included in the integration (Orszag 1970; Gordon and Stern 1982). When the atmospheric data is transformed from spectral space to real space for the purposes of analysis, this resolution results in a grid box size of about 4.5° lat × 7.5° long. In the vertical, finite differencing is used at nine unevenly spaced levels. The radiative transfer calculation includes the effects of clouds, water vapor, carbon dioxide, and ozone on both incoming and outgoing radiation. The sky is overcast whenever the relative humidity exceeds a critical level; otherwise clear sky is predicted. While the distribution of water vapor is predicted by the model, carbon dioxide concentration is taken to be constant, except in the global warming experiments described below. Ozone is specified as a function of latitude, height, and time of year, following observations given by Hering and Borden (1965). At the land surface, the model computes budgets of snow, water, and heat. Soil moisture is parameterized using a "bucket" model: At every land surface grid point, water is accumulated through precipitation and depleted through evaporation in a bucket whose surface area is the same as the grid box. At any given time, if the water depth in the bucket exceeds 15 cm, runoff is predicted. Otherwise, soil moisture is given by the depth of the water in the bucket.

The finite-difference oceanic component, with a horizontal resolution of 4.5° lat × 3.75° long and 12 vertical levels, uses the modular ocean model (MOM) code described in Pacanowski et al. (1991). This particular version of MOM is based, in turn, on a model described by Bryan and Lewis (1979). In addition to horizontal and vertical background subgrid-scale mixing, the model has isopycnal mixing as discussed by Redi (1982) and Tziperman and Bryan (1993). Convection occurs whenever the vertical stratification becomes unstable.

Sea ice is predicted using a free drift model developed by Bryan (1969).

At the beginning of time integration, the model's atmosphere and ocean are both individually in equilibrium with realistic seasonal and geographical distributions of sea surface temperature, sea surface salinity, and sea ice. However, as the integration proceeds, the model's climate usually drifts toward its own, less realistic, equilibrium state. This distorts the simulated variability that this study seeks to diagnose. Moreover, it would be difficult to interpret a global warming experiment where the radiative forcing perturbation is applied to a basic-state climate that is already diverging significantly from the present-day equilibrium state. Therefore, to minimize the climate drift, the fluxes of heat and water obtained from the atmospheric component of the coupled model are modified by given amounts before they are imposed upon the ocean surface. While these adjustments vary seasonally and geographically, they do not vary from year to year. Therefore, they are not correlated to the transient sea surface temperature and salinity anomalies that develop over the course of the coupled integration. Thus flux adjustment is unlikely either to amplify or damp these anomalies in a systematic way. Although the adjustments do not eliminate the shortcomings of the model (Marotzke and Stone 1995), they do prevent rapid drift of the simulated climate from realistic initial conditions. Using this flux adjustment technique, only very small trends associated with climate drift remain. For example, over the entire period of the 1000-yr integration, the fixed H₂O run exhibits a cooling trend of 0.009°C century⁻¹ in global-mean surface temperature. A trend of a similar magnitude exists in the 1000-yr control run (0.035°C century⁻¹). For the purposes of the analysis of the model's unperturbed variability, all such linear trends were first removed from the data.

3. Experimental design

As noted in section 1, this model was integrated in two configurations to test the effects of water vapor feedback. In both cases, water vapor is variable in the hydrologic component of the model, meaning that simulated clouds and precipitation are based on humidity values predicted by the model. In the fixed H₂O configuration, however, water vapor mixing ratios at all grid points and all nine vertical levels are fixed to their climatological mean, seasonally varying values in the longwave portion of the radiative transfer subroutine. In the control configuration, on the other hand, the water vapor values predicted by the hydrologic component are passed to the longwave subroutine. The mean water vapor field used in the fixed H₂O experiments was calculated in the following way. First, integrating only the atmospheric component of the coupled model, and using seasonally varying, climatological sea surface temperatures and sea ice as a lower boundary condition, the

daily mean values of the entire water vapor field were saved away for 50 yr. Then the values corresponding to any given day of the annual cycle were averaged over all 50 yr of the integration, providing a mean water vapor field for every day of the year. These mean values were supplied to the coupled model's longwave radiative transfer subroutine as the coupled integration proceeded through each day of the year.

It should be emphasized that since water vapor was fixed only in the longwave radiative transfer subroutine of the fixed H₂O configuration, any feedback effects due to water vapor's interaction with solar radiation are included in both configurations. The aspect of water vapor feedback relating to solar radiation is therefore not a subject of this study. However, it also constitutes a positive feedback mechanism, since water vapor absorbs solar radiation. For example, a warm surface-troposphere temperature anomaly will increase the amount of water vapor in the atmosphere and enhance the absorption of solar radiation there, thereby amplifying the warm anomaly. If we had fixed water vapor in the solar radiative transfer subroutine as well as the long wave, the fixed H₂O experiment would have had even less positive feedback and therefore less unperturbed variability and a smaller response to a doubling of CO₂. However, this effect is quite small; the impact of the shortwave component of water vapor feedback, though positive, is approximately an order of magnitude smaller than the longwave component (Ramanathan and Coakley 1978). For the sake of simplicity, the term "water vapor feedback" refers only to the longwave feedback effects of water vapor throughout this article.

The model was integrated for 1000 yr in each configuration. These integrations will be referred to as the unperturbed variability experiments. The last 800 yr of these time series were used to analyze the effects of water vapor feedback on the model's internally generated variability. The global warming experiments were initialized using the same initial conditions as the two unperturbed variability experiments. Integrating the model in both configurations, CO₂ was then increased at a rate of 1% per year until its concentration doubled, around year 70. Thereafter it was fixed at the doubled value (720 ppm) for the remainder of the 500-yr-long experiments.

4. Spatial and timescale dependence of water vapor feedback in unperturbed variability

As mentioned in section 1, one goal of this study is to understand the spatial and timescale dependence of water vapor feedback in the unperturbed temperature variability of the surface-troposphere system. Does the contribution of water vapor feedback depend upon the geographical extent of the temperature anomaly? Does it depend on how long the anomaly persists? To simplify the analysis, we selected a single variable—surface temperature—that would be broadly representative of the

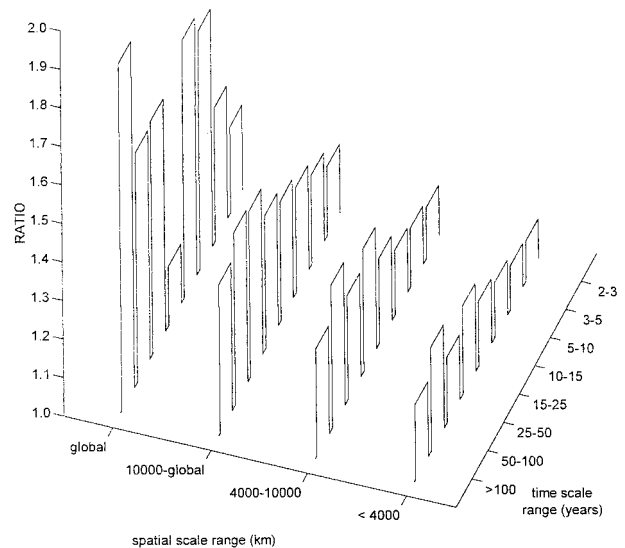


FIG. 1. The ratio control/fixed H₂O of the standard deviation of surface temperature anomalies, indicated by the heights of the bars, as a function of spatial scale and timescale. The ranges of time- and spatial scales selected for the analysis are shown in the figure. The spatial filtering required for the calculation of these ratios was performed in the following way. First, spatial filtering was carried out on the model's 48 × 40 grid using a Hamming digital filter in the zonal direction and a Fourier filter in the meridional direction. To select the same spatial scales at all latitudes, the digital filter varied by latitude row, taking into account the reduction in the length of a latitude circle as higher latitudes are chosen. Applying the filters in both the zonal and meridional directions to global fields of surface temperature anomalies, a new time series was produced at each grid point.

impact of water vapor feedback on these anomalies. Thus to answer these questions we compare the surface temperature variability in the fixed H₂O 1000-yr run to the control 1000-yr run on various spatial scales and timescales. Since water vapor feedback is present in the control case but absent in the fixed H₂O case, differences in variability may be ascribed to water vapor feedback. Using the following technique, it was possible to focus on any given range of spatial scales and timescales. First, the temperature anomalies of the spatial scales of interest, from 4000 to 10 000 km, for example, were selected by applying the appropriate filter in the zonal and meridional directions to each field of annual-mean temperature anomalies. Similarly, the variability corresponding to a given range of timescales, from 10 to 15 yr, for example, was extracted by bandpass filtering the resulting time series at each grid point. After applying this series of filters to both the control and fixed H₂O time series, the variability of the filtered control time series was compared to its fixed H₂O counterpart by taking the ratio of the control to fixed H₂O standard deviations at each grid point. Figure 1 depicts graphically how the global mean of this ratio changes as various spatial scales and timescales are selected. In addition, to study the role of water vapor feedback on the largest (i.e., global) spatial scale, global-mean surface

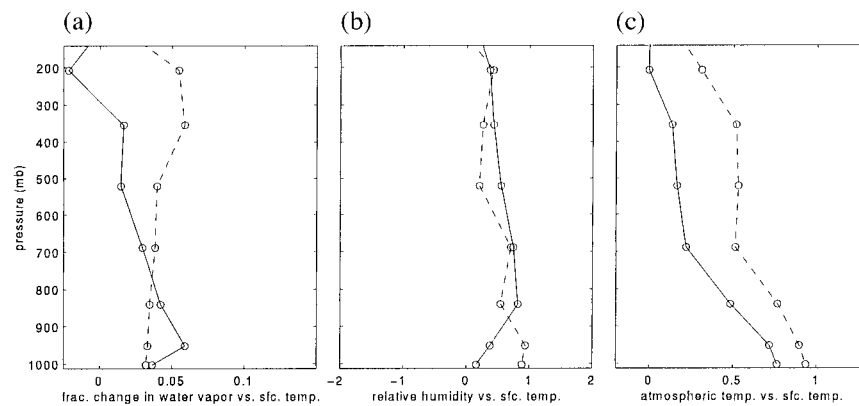


FIG. 2. The regressions between (a) fractional changes in water vapor mixing ratios and surface temperature ($^{\circ}\text{C}$), (b) relative humidity (%) and surface temperature, and (c) troposphere temperature and surface temperature in the seven lowest levels of the model (142–1013 hPa) for local (solid) and global (dashed) cases.

temperature time series were calculated for both runs. These two time series were bandpass filtered at various timescales and the variability in the control run was compared to the fixed H_2O run by taking the ratio of the two standard deviations. These ratios are also plotted in Fig. 1 for comparison with smaller spatial scales.

Two conclusions may be drawn from this figure. First, the ratio is greater than one for all time- and spatial scales, implying that there is more surface temperature variability in the control run than in its fixed H_2O counterpart on all time and spatial scales. Thus water vapor feedback is a positive feedback mechanism that enhances the internally generated surface temperature variability of this model. Second, the ratio increases as larger spatial scales and longer timescales are selected. For example, in the case of the small spatial-scale anomalies (spatial scale < 4000 km), the ratio increases from 1.10 for the 2–3-yr timescale to 1.19 for the longest timescales (> 100 yr). More importantly, the ratio generally increases very dramatically the larger the spatial scale in question. For example, on the 5–10-yr timescale, the ratio increases from 1.14 for anomalies smaller in spatial scale than 4000 km, to 1.62 for global-mean anomalies. On the longest timescales (> 100 yr) the ratio increases from 1.19 for small-scale anomalies to 1.90 in the global-mean case.

Since water vapor feedback is a positive feedback mechanism in unperturbed variability, tropospheric absolute humidity must increase (decrease) as surface temperature increases (decreases). This relationship results from the fact that the saturation mixing ratio of water vapor increases exponentially with temperature. Thus a temperature anomaly in the surface–troposphere system is associated with an anomaly of the same sign in the water-vapor-holding capacity of the atmosphere. If condensation in the troposphere and evaporation from the surface act to keep relative humidity approximately constant throughout the troposphere, then absolute humidity levels will fluctuate in phase with surface–troposphere

temperature. By testing this reasoning, we aim to explain, at least in part, the most important result from Fig. 1: that water vapor feedback is more effective at large spatial scales than small.

The argument outlined above depends on the relationships between three tropospheric variables and surface temperature: absolute humidity, relative humidity, and air temperature. Accordingly, Fig. 2 shows the regressions at every level of the model's troposphere between these variables and surface temperature. All calculations are based on annual-mean data from the control unperturbed variability experiment. To clarify how each of these quantities responds to large- and small-scale surface temperature anomalies, the regressions were calculated for two cases. In all three panels, the regressions between global-mean atmospheric variables and global-mean surface temperature are shown with a dashed line, while the global means of the local regressions, calculated separately at every grid point, are shown with a solid line. Thus the dashed lines represent the relationships between surface temperature and absolute humidity, relative humidity, and air temperature, and on the largest (global) spatial scale. On the other hand, the solid lines show how, on average, local fluctuations in these quantities relate to changes in local surface temperature. Of course, local anomalies include contributions from all spatial scales larger than a grid box, including the global scale. However, the variability at a single grid point is overwhelmingly dominated by fluctuations smaller in spatial scale than the global scale. For example, in the control unperturbed variability experiment, the global-mean standard deviation of local surface temperature is about 0.74°C , whereas the standard deviation of global-mean surface temperature is only about 0.13°C . Since the magnitude of a typical global anomaly is so much smaller than the magnitude of a typical local anomaly, fluctuations smaller in spatial scale than the global scale must be responsible for most local variability. We may therefore consider the regres-

sions shown by solid lines to represent relationships between atmospheric variables and surface temperature at spatial scales much smaller than the global scale.

We begin the discussion of these results by focusing on Fig. 2a. Regressions were calculated using fractional changes in absolute humidity, rather than absolute humidity itself, to focus directly on the impact of water vapor fluctuations on the radiative properties of the atmosphere. Since longwave absorptivity due to water vapor is approximately proportional to the logarithm of the water vapor mixing ratio in the troposphere, fractional changes in water vapor are roughly proportional to changes in atmospheric absorptivity due to water vapor. Figure 2a illustrates water vapor feedback's greater impact on large spatial scales than small in terms of this relationship. In the lower troposphere, the strength of the global-scale relationship between absorptivity due to water vapor and surface temperature is not significantly different from that of the local anomalies. However, in the mid- to upper troposphere, the situation is very different. Here, the global-scale relationship is much stronger than its local counterpart. Because of the proximity to the top of the atmosphere, changes in absorptivity here probably have a larger effect on the atmosphere's greenhouse effect than if a similar change were to occur in the lower troposphere. In any case, when the entire troposphere is considered, a given global-mean temperature anomaly induces a larger fractional increase in water vapor in the air column above than a typical local anomaly of the same magnitude.

But why are the fractional changes in water vapor per degree change in surface temperature larger in the global than the local case? Figure 2b shows that relative humidity changes very little as surface temperature fluctuates; the regressions are nearly zero throughout the troposphere for both local and the global cases. This indicates that neither local nor global surface temperature anomalies are associated in any systematic way with anomalies in relative humidity in the troposphere. The differing relationships between absolute humidity and surface temperature must therefore be explained by differences in the relationships between tropospheric temperature and surface temperature, as illustrated in the right panel. This panel shows that global-scale surface temperature anomalies penetrate much more deeply into the troposphere than their local counterparts. This is most apparent in the upper troposphere, where the regressions between atmospheric temperature and surface temperature in the global case are nearly four times as large as in the local case. Given that the same surface temperature anomalies induce virtually no change in relative humidity, this implies a larger change in absolute humidity in the global case.

The results presented in Fig. 2 explain how water vapor feedback's contribution to the radiative damping of temperature anomalies depends on their spatial scale. However, temperature anomalies of the surface-troposphere system may also be damped by horizontal ex-

change of sensible heat within the atmosphere itself. The effectiveness of this process also depends on the anomalies' spatial scale. For example, a small-scale temperature anomaly would be very effectively diffused into surrounding regions by horizontal advective heat exchange. Clearly, this diffusive damping of temperature anomalies is less effective the larger the anomaly's spatial scale. At the global scale, of course, it is nonexistent. Since water vapor feedback operates exclusively on the radiative component of the damping, the impact of water vapor feedback on small spatial scales may be smaller simply because the relative contribution of radiative damping to the total damping is smaller. This constitutes another explanation for the spatial scale dependence of the ratio plotted in Fig. 1. It should also be pointed out that advective processes in the atmosphere are also the main reason why the regressions of local atmospheric temperature and surface temperature, shown in Fig. 2c, are smaller than their global-mean counterparts. This, in turn, is responsible for the weaker water vapor feedback in the case of the local anomalies. Thus advection not only contributes heavily to the damping of small-scale surface temperature anomalies, obscuring the effects of water vapor feedback, but it also weakens water vapor feedback itself.

Temperature anomalies are damped by evaporative fluxes across the air-surface interface as well. This process is also likely to be more effective at small spatial scales due to the increasing effects of advection as spatial scales decrease. For example, while a warm global-scale anomaly may be associated with enhanced evaporation at the surface, this latent heat must ultimately be released in the atmosphere. This would result in an enhancement of the warm anomaly in the troposphere, which must in turn warm the surface through enhanced radiative and sensible heat fluxes, counteracting the cooling effect of the initial evaporative flux. The net damping effect of the evaporative flux on the global-mean surface-troposphere temperature anomaly is therefore limited. A small-scale warm anomaly would also result in enhanced evaporation. Although this latent heat must be released somewhere in the atmosphere, it may be released at a different location, resulting in an export of heat out of the region of the anomaly. In this case, the effect of the initial evaporative flux at the surface would be to damp the entire surface-troposphere anomaly. Thus evaporative damping may also obscure the effects of water vapor feedback at small scales by decreasing the relative contribution of radiative processes to the total damping.

We have seen how and why water vapor feedback affects internally generated surface temperature variability on various spatial scales. We now verify that water vapor feedback actually alters the top-of-the-atmosphere, longwave radiative damping of these anomalies in a manner consistent with its impact on their variability. The first row of the first column of Table 1 shows the regression between global-mean, clear-sky

TABLE 1. The regressions between global-mean clear-sky outgoing longwave radiation and global-mean surface temperature (first row) and the global-mean of the regressions between local clear-sky outgoing longwave and local surface temperature (second row). The third column shows the difference in the regressions between the control and fixed H₂O cases.

| | Control | Fixed H ₂ O | Difference |
|-------------------------------------|---------|------------------------|------------|
| Global anomalies | | | |
| W m ² (°C) ⁻¹ | 1.97 | 2.69 | 0.72 |
| Local anomalies | | | |
| W m ² (°C) ⁻¹ | 1.42 | 1.92 | 0.50 |

outgoing longwave radiation and global-mean surface temperature for the control unperturbed variability experiment. Immediately below is the global-mean of the regressions between local clear-sky outgoing longwave and local surface temperature. These two values represent the change in the clear-sky longwave flux at the top of the atmosphere per unit change in surface temperature on both the local and the global scale. This is a measure of the strength of the radiative damping of surface temperature. By examining clear-sky fluxes, we eliminate the effects of cloud feedback. The second column presents the results of the same calculations for the fixed H₂O experiment. Finally, the third column shows the difference in the regressions between the control and fixed H₂O cases. In both the local and the global cases, the regressions are larger for the experiment without water vapor feedback; the presence of water vapor feedback in the control experiment reduces the longwave damping of both local and global temperature anomalies. In the global case, water vapor feedback reduces the damping by 0.72 W m⁻² °C⁻¹, the difference between the two regressions, whereas in the local case, the damping is reduced by 0.50 W m⁻² °C⁻¹. The reduction is larger for the global-mean case, which is consistent with the observation that water vapor feedback is more effective the larger the spatial scale.

5. Water vapor feedback and global warming

We wish to examine the role of water vapor feedback in global warming as well as unperturbed variability. As described in section 3, global warming experiments were performed integrating the model in both configurations. Carbon dioxide was increased starting at the beginning of the two integrations a rate of 1% yr⁻¹ until its concentration doubled around year 70. Thereafter it was fixed at its doubled value (720 ppm). Just as in the analysis of unperturbed variability presented in section 4, we analyzed surface temperature to diagnose the climate change in the two experiments. Figure 3 shows the 500-yr annual-mean time series of the global-mean surface temperature change in these integrations relative to the unperturbed variability experiments, where CO₂ is fixed at 360 ppm. In both the fixed H₂O and control cases, there is a steady warming for the first 70 yr. After year 70, the warming continues but at a much slower

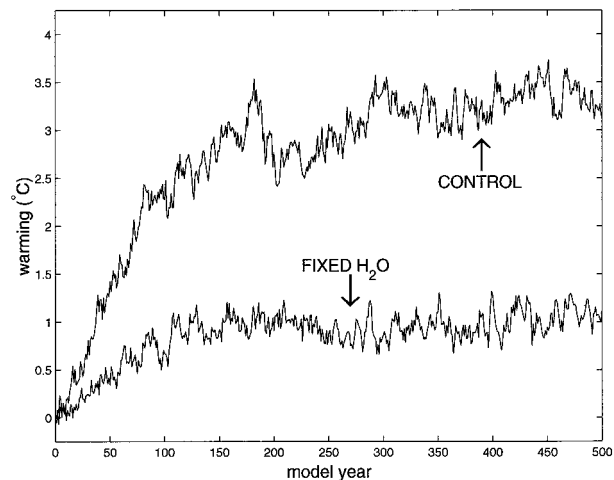


FIG. 3. The 500-yr annual-mean time series of the global-mean surface temperature change in the integrations where CO₂ is doubled to 720 ppm relative to the unperturbed variability experiments, where CO₂ is fixed at 360 ppm.

rate for the remainder of the experiments. If the integrations were continued beyond year 500, both climates would likely continue to change slowly for several centuries in response to the new CO₂ value. However, enough of the climate change has occurred by this point that we may consider the climates toward the end of these integrations to be broadly representative of their equilibrium response to the increase in CO₂. It is clear from the figure that the magnitude of the warming is much larger in the model that contains water vapor feedback than the model that does not: The warming averaged over the last century of the integrations is 3.38°C in the control case, while it is only 1.05°C in the fixed H₂O case.

These results demonstrate that water vapor feedback is positive in the global warming case just as it is positive in the context of unperturbed variability. However, the amount by which water vapor feedback amplifies global warming is larger than the amount by which it amplifies the magnitude of a typical internally generated surface temperature anomaly. Since standard deviation is a measure of the magnitude of a typical anomaly, this may readily be seen by comparing the ratio (control/fixed H₂O) of standard deviation of surface temperature to the ratio of the warming. If water vapor feedback is equally effective in both, then the ratios should be identical. Since CO₂-induced warming occurs on a global scale, and because of the spatial-scale dependence of water vapor feedback documented in section 4, we compare the warming ratio to the ratio of standard deviation of global-scale temperature fluctuations. The warming ratio is 3.38°C/1.05°C = 3.2. However, the ratio of standard deviation of global-mean, annual-mean surface temperature is 1.53. Thus water vapor feedback is more than twice as effective in enhancing global warming as

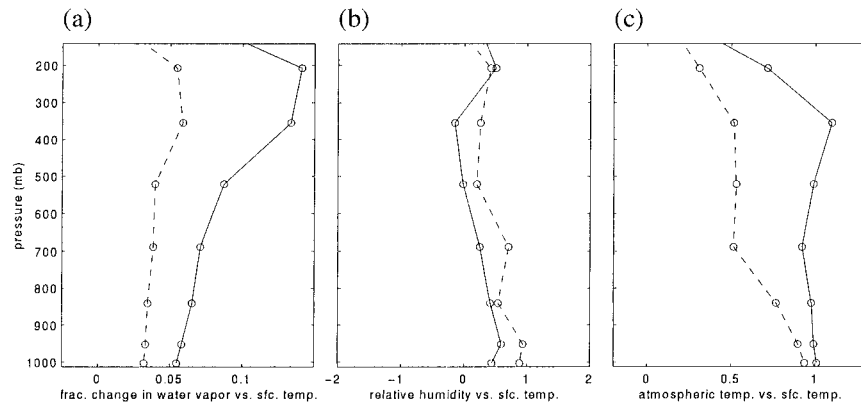


FIG. 4. As in Fig. 2, (a) the relationships between fractional changes in water vapor and surface temperature ($^{\circ}\text{C}$), (b) the relationships between relative humidity (%) and surface temperature, and (c) the relationships between tropospheric temperature ($^{\circ}\text{C}$) and surface temperature. In all three panels, the solid lines indicate the relationships between atmospheric variables and surface temperature for the global warming case. The dashed lines show the regressions between global-mean values and global-mean surface temperature from the control unperturbed variability experiment. Note that Fig. 4 has the same aspect ratio and axes as Fig. 2.

it is in amplifying internally generated, global-mean temperature anomalies.

In section 4 we explained why the effectiveness of water vapor feedback depends on spatial scale by examining the relationships between surface temperature on the one hand and fractional changes in absolute humidity, relative humidity, and tropospheric temperature on the other. Using identical methods, we now explain why water vapor feedback is so much more effective in global warming than unperturbed variability. In direct analogy to Fig. 2, Fig. 4 shows the relationships between fractional changes in water vapor and surface temperature, relative humidity and surface temperature, and tropospheric temperature and surface temperature. All of the dashed curves indicate regressions between global-mean, annual-mean values from the control unperturbed variability experiment. They are therefore identical to the dashed curves in Fig. 2. The solid lines, while not regressions, indicate the analogous relationships between atmospheric variables and surface temperature for the global warming case. In the case of atmospheric temperature (right panel), these values were calculated by subtracting the global-mean tropospheric temperatures averaged over years 401–500 of the control unperturbed variability experiment from the global-mean tropospheric temperatures averaged over years 401–500 of the control global warming experiment. The differences were then divided by the difference in global-mean surface temperature averaged over the same time period. The resulting ratios therefore represent the warming that takes place in the troposphere per degree surface temperature warming, just as the regressions represented by the dashed lines indicate the tropospheric temperature changes that take place per degree surface temperature fluctuation. The relationships between relative humidity and surface temperature (middle panel)

were calculated in a similar fashion. The values indicated by the solid line in the left panel were calculated by first taking the difference between the global-mean mixing ratios averaged over years 401–500 of the control global warming and unperturbed variability experiments and dividing by the average mixing ratios from the unperturbed variability experiment. Finally, these fractional changes in water vapor were divided by the difference in global-mean surface temperature between the two experiments.

First, we compare the relationships between the fractional changes in water vapor and surface temperature for global-scale unperturbed variability and the global warming, shown on the left in Fig. 4. As described in section 4, this is approximately equivalent to analyzing the relationship between atmospheric absorptivity due to water vapor and surface temperature. At all levels of the troposphere, there is a strong positive relationship between fractional changes in water vapor and surface temperature for both the unperturbed variability and global warming cases. However, for a given change in surface temperature, a much larger fractional change in water vapor occurs in the global warming case. Although this is true at all levels of the troposphere, it is most apparent in the upper troposphere, where changes in absorptivity probably have a larger effect on the atmosphere's greenhouse effect than if a similar change were to occur in the lower troposphere. This evidence is consistent with the fact that water vapor feedback is more effective in enhancing global warming than in amplifying internally generated, global-mean anomalies.

We have already established that, throughout the troposphere, there is no systematic relationship between internally generated, global-mean relative humidity and surface temperature anomalies. The middle panel of Fig.

4 shows that relative humidity also changes very little as the surface warms in response to increased CO_2 . There is a very small increase of a few tenths of a percent per degree warming in the lower troposphere, while in the mid- to upper troposphere, the relationship falls off nearly to zero. Thus in both the unperturbed variability and global warming cases, surface temperature anomalies have very little effect on tropospheric relative humidity.

Given that the relative humidity anomalies associated with surface temperature anomalies are small in both unperturbed variability and global warming cases, the degree to which a surface temperature anomaly penetrates the troposphere must be a critical factor in determining the strength of the water vapor feedback. We now examine both the vertical structures of the warming in the global warming experiment and temperature anomalies in the unperturbed variability experiment, shown in Fig. 4c. In both cases, there is a strong relationship between temperature anomalies aloft and temperature anomalies at the surface. However, the relationship is much stronger in the global warming case, where the warming is nearly uniform throughout the entire troposphere. In the unperturbed variability case, on the other hand, the regression between tropospheric temperature and surface temperature decreases from almost 1 near the surface to about 0.3 at 200 hPa. Internally generated, global-mean temperature anomalies do not penetrate as effectively into the troposphere as warming induced by a doubling of CO_2 . Thus for a CO_2 -induced warming and an internally generated warm anomaly of the same magnitude, the fact that relative humidity changes very little in both cases implies a much larger increase in upper-tropospheric water vapor mixing ratios in the global warming case than the unperturbed variability case. This implies a stronger water vapor feedback to global warming.

Since the degree to which a surface temperature anomaly penetrates the troposphere is such a critical factor in determining the strength of its associated water vapor feedback, it is desirable to gain an understanding of why internally generated, global-mean temperature anomalies do not penetrate as effectively into the troposphere as the warming induced by a doubling of CO_2 . To shed light on this issue, we examined the characteristic horizontal structure of both global-scale unperturbed temperature variability and global warming at every level of the model's troposphere. To see how the characteristic horizontal structure of internally generated, global-mean temperature anomalies changes with height, we calculated regressions between local and global-mean temperature at each level of the troposphere using annual-mean data from the control unperturbed variability experiment. To simplify the presentation of these results, we then computed the mass-weighted average of these regressions over two layers of the troposphere, one corresponding to the lower troposphere (770–1013 hPa), and the other corresponding

to the mid- and upper troposphere (273–770 hPa). The geographical distribution of these regressions for both layers is shown in Fig. 5. The patterns for both layers are very similar to the patterns for their constituent levels and are therefore broadly representative of the change with height in the horizontal structure of global-mean temperature anomalies. We also performed an analogous calculation for the global warming case. We first computed the warming due to a doubling of CO_2 at each grid point and each vertical level of the troposphere by taking the difference in temperature between the control global warming and unperturbed variability experiments averaged over the fifth century of both integrations. Then, at each vertical level, we divided these values by the global-mean warming at that level. Finally, we calculated the mass-weighted average of these ratios over the lower (770–1013 hPa) and mid- to upper (273–770 hPa) troposphere, as before. The geographical distribution of these values is shown in Fig. 6.

We begin the discussion of these calculations by examining the unperturbed variability case. Figure 5b reveals that global-mean temperatures in the lower troposphere are dominated by contributions from midlatitude land locations, the high latitudes of the Southern Hemisphere, and a region stretching from the equatorial to the southeastern tropical Pacific. Thus when global-mean lower-tropospheric temperature is anomalously warm, these regions also tend to be warm. The regression pattern for surface temperature (not shown) is very similar. At the same time, Fig. 5a shows that when global-mean temperatures in the upper troposphere are warm, temperatures in other regions—mainly a wide band stretching across nearly the entire world from 30°N to 30°S—tend to be warm. Thus the regions contributing most to global-mean variability shift markedly as one goes from the surface and lower troposphere to the mid- and upper troposphere. Temperature variability in the regions that dominate the mid- and upper-tropospheric global-mean variability is most likely only weakly related to the variability in the distant regions that dominate the global-mean variability at the surface and in the lower troposphere. This explains the substantial decrease with height in the regression between global-mean tropospheric temperature and surface temperature seen in the dashed line of Fig. 4c.

A very different picture emerges from the global warming case. Figure 6b shows that, in the lower troposphere, warming is larger than the global-mean value in the mid- to high latitudes of both hemispheres, while it is less than the global-mean value in much of the midlatitudes and Tropics. The ratio pattern at the surface (not shown) is very similar. Figure 6a also reveals a similar pattern for the mid- and upper troposphere, although the equator-to-pole contrast in the ratio is somewhat smaller. Thus where warming is large at the surface and in the lower troposphere, it is also large in the mid- and upper troposphere. This confirms that the uniform global-mean tropospheric warming seen in the solid line

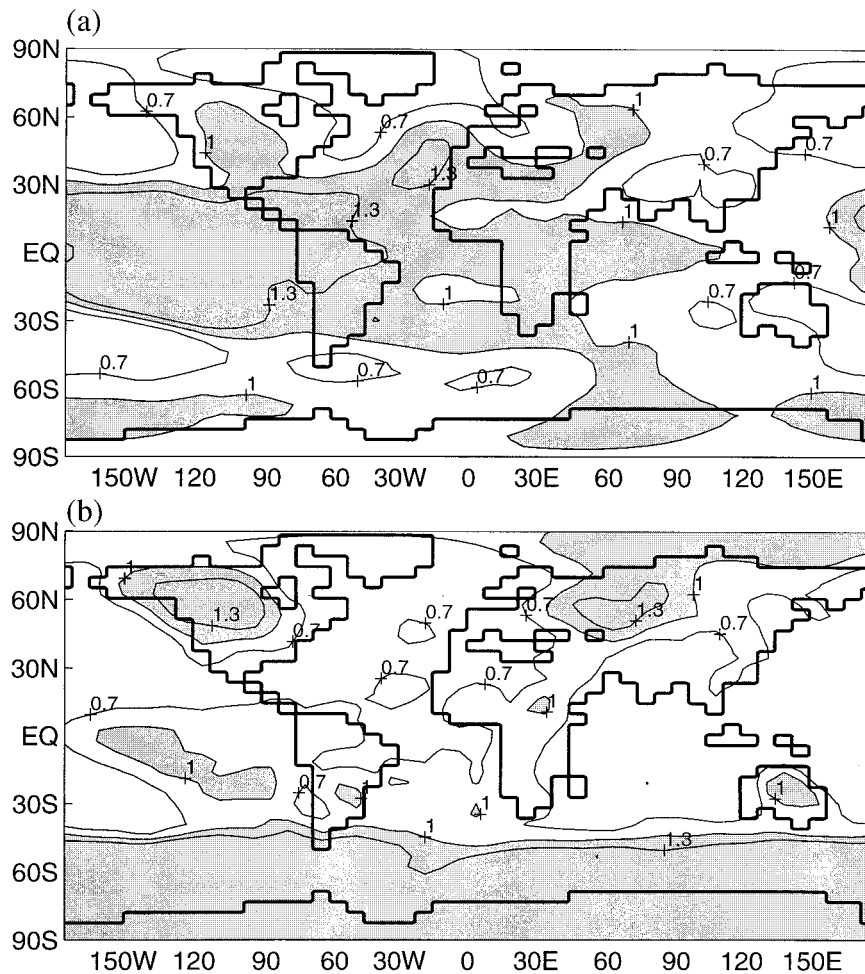


FIG. 5. The geographical distribution of the mass-weighted, vertically averaged regressions between local and global-mean temperature from the control unperturbed variability experiment for two cases. (a) Averaged over the mid- to upper troposphere (273–770 hPa). (b) Averaged over the lower troposphere (770–1013 hPa). Regions where the regressions exceed 1 are shaded.

of Fig. 4c also has a horizontal structure that is uniform with height. A warming at a given location is associated with a very similar warming aloft and therefore induces a large water vapor feedback. This is because global warming is the climate response to a steady, globally uniform forcing. Conversely, internally generated, global-mean temperature anomalies are a superposition of many modes of variability, whose individual impact is not geographically uniform, and that may not affect all parts of the troposphere equally. Thus the horizontal structure of an internally generated, global-mean anomaly does not persist as height increases and the water vapor feedback to such an anomaly is accordingly weaker.

6. Interaction between water vapor and other feedbacks

In section 5, we showed that water vapor feedback amplifies the model's global warming response to a

doubling of CO_2 by a factor of 3.2. This is substantially greater than previous estimates of the impact of water vapor feedback. For example, Manabe and Wetherald (1967) showed that a radiative-convective model where relative humidity is fixed (analogous to our control model) was about twice as sensitive to an external forcing as a fixed absolute humidity model (analogous to our fixed H_2O model). Using nearly identical techniques, other modeling studies have arrived at similar results (see Ramanathan and Coakley 1978): water vapor feedback amplifies the climate response to an external forcing by approximately a factor of 2. Extrapolating from Raval and Ramanathan's (1989) observational estimate of the strength of water vapor feedback, Cess (1989) calculated that water vapor feedback would amplify CO_2 -induced global warming by a factor of about 1.6. Although this calculation may not be perfectly accurate, since Raval and Ramanathan's estimate is based on the geographical variation of water vapor and surface temperature during only one month,

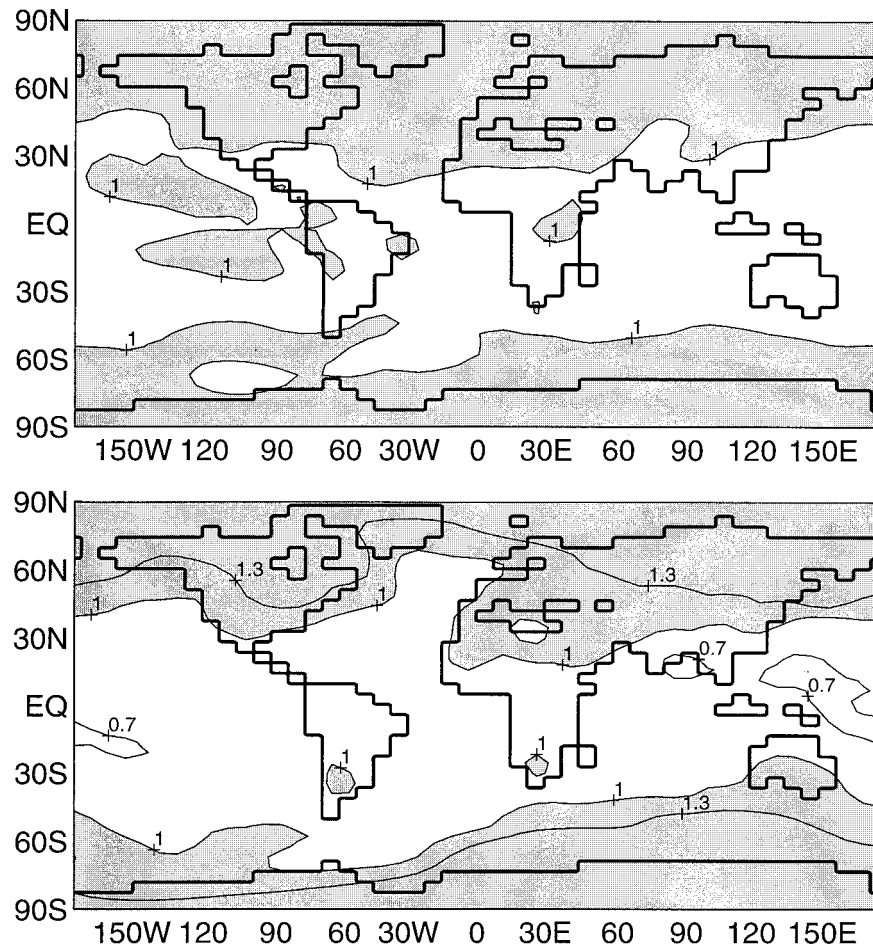


FIG. 6. The geographical distribution of the mass-weighted, vertically averaged ratio between local and global-mean warming due to CO₂ doubling for two cases. (a) Averaged over the mid-to upper troposphere (273–770 hPa). (b) Averaged over the lower troposphere (770–1013 hPa). Regions where the ratio exceeds 1 are shaded.

it is nevertheless much lower than 3.2. In this section, we explain the discrepancy between our estimate of water vapor feedback’s impact and those of previous studies.

The interaction between water vapor feedback and other feedback mechanisms is not taken into account in any of the above-mentioned studies. However, the model considered here does contain other feedback mechanisms, such as albedo and cloud feedback, that alter the impact of water vapor feedback. We may illustrate this point mathematically. Let T'_c be the equilibrium global warming response of the control model to a thermal forcing Q . Response T'_c can be related to Q through the sensitivity parameter of the control climate, Λ_c :

$$T'_c = \frac{Q}{\Lambda_c}. \tag{1}$$

An identical relationship exists among the equilibrium global warming response in the fixed H₂O model

(T'_f), the same thermal forcing Q , and the sensitivity parameter of the fixed H₂O climate, Λ_f :

$$T'_f = \frac{Q}{\Lambda_f}. \tag{2}$$

Thus the ratio of the warming in the two climates equals the inverse ratio of the sensitivities:

$$\frac{T'_c}{T'_f} = \frac{\Lambda_f}{\Lambda_c}. \tag{3}$$

We may rewrite Eq. (3) by expanding the sensitivity parameters in terms of contributions from various feedback mechanisms:

$$\frac{T'_c}{T'_f} = \frac{\Lambda_f}{\Lambda_c} = \frac{\lambda_o - \sum_f \lambda}{\lambda_o - \lambda_{w,lw} - \sum_c \lambda}. \tag{4}$$

Here λ_o represents the climate sensitivity parameter

that would result if no feedback mechanisms were in effect. This value is the change in outgoing longwave per degree centigrade that results from the temperature increase alone, as given by the Stefan–Boltzmann law. The mean climate for the two experiments prior to CO₂ doubling is nearly identical, so λ_o may be taken to be the same for both experiments. The variable $\lambda_{w,lw}$, which applies only to the control model, is the change to λ_o owing to the longwave effects of water vapor feedback. Here, $\Sigma_c \lambda$ and $\Sigma_f \lambda$ are the modifications to λ_o that arise from the other feedback mechanisms in the control and fixed H₂O models, respectively. They each include contributions from albedo, cloud, and lapse rate feedbacks, which may not have the same strength in the two models.

We now divide both the numerator and the denominator of equation 4 by λ_o , which gives the contributions of feedback mechanisms to the two climate sensitivities in terms of nondimensional gain factors:

$$\frac{T'_c}{T'_f} = \frac{1 - \sum_f g}{1 - g_{w,lw} - \sum_c g}. \quad (5)$$

It is clear from Eq. (5) that impact of water vapor feedback, as measured by the ratio of the warmings, is affected not only by $g_{w,lw}$, the nondimensional longwave water vapor feedback parameter, but also by the contributions of other feedback mechanisms, as given by $\Sigma_c g$ and $\Sigma_f g$. For this reason, it is desirable to understand how all feedback mechanisms contribute to the sensitivities of the control and fixed H₂O climates. In so doing, we aim to explain why our estimate of water vapor feedback's impact is so much larger than previous estimates.

To carry out this quantitative evaluation of all feedback mechanisms, we calculated the radiative effects of the simulated changes in lapse rate, water vapor, cloudiness, and surface albedo upon CO₂ doubling using an off-line version of the model's radiative transfer subroutine. Starting with the temperature, water vapor, cloudiness, and surface albedo distributions averaged over years 401–500 of the unperturbed variability experiments, we calculated the global-mean net incoming solar and outgoing longwave radiation at the top of the atmosphere. Then, to focus on a particular feedback mechanism, we performed a second off-line calculation. For example, to assess the control model's albedo feedback, we imposed the mean surface albedo averaged over years 401–500 of the control global warming experiment and recalculated the net incoming global-mean solar radiation at the top of the atmosphere. We then divided the change in net incoming solar radiation resulting from the surface albedo decrease by the global-mean surface temperature change due to CO₂ doubling (3.38°C). This gave λ_a , the contribution of albedo feedback to the $\Sigma_c \lambda$ terms shown in Eq. (4). Finally, we divided λ_a by λ_o , calculated based on the global-mean

TABLE 2. The gain factors for lapse rate, water vapor, cloud, and surface albedo feedbacks as calculated using the off-line radiation code.

| | Control | Fixed H ₂ O |
|-------------------------|---------|------------------------|
| Lapse rate (g_{lr}) | 0.17 | 0.24 |
| Water vapor (g_w) | 0.39 | 0.07 |
| Cloud (g_c) | 0.14 | 0.10 |
| Sfc. albedo (g_a) | 0.12 | 0.11 |
| Correction | 0.01 | −0.00 |

emission temperature of the model climate. This gave the gain factor g_a for albedo feedback. An analogous calculation was carried out for cloud and water vapor feedback. To quantify lapse rate feedback, the increase in global-mean outgoing longwave radiation at the top of the atmosphere due to the CO₂-induced temperature change was divided by the temperature increase itself. This value was then subtracted from λ_o , the change in outgoing longwave radiation per degree Kelvin expected from the Stefan–Boltzmann law, thereby isolating the effects of CO₂-induced changes in the vertical temperature structure. The entire procedure was repeated for the fixed H₂O case for all feedbacks, except that the change in water vapor upon CO₂ doubling was not allowed to affect longwave radiation in the assessment of water vapor feedback.

The resulting values for the gain factors are shown in Table 2. The gain factors for lapse rate feedback are quite large in both models due to the large stratospheric cooling that occurs when CO₂ doubles. This reduces outgoing longwave radiation at the top of the atmosphere, thereby making lapse rate feedback positive. The gain factor is somewhat larger in the fixed H₂O case because the stratospheric cooling is nearly identical in both models, so that the reduction in outgoing longwave radiation on a per degree centigrade basis is larger in the experiment with less warming. The fact that lapse rate feedback is positive and has a stronger effect in the model without water vapor feedback is a consequence of our choice to analyze the changes in radiative fluxes due to feedback mechanisms at the top of the atmosphere, rather than at the tropopause, as is often done. This unfortunately combines the effects of CO₂-induced stratospheric cooling, which is not normally thought of as contributing to lapse rate feedback, and tropospheric lapse rate changes, which are. However, we were compelled to choose the top of the atmosphere as our reference level because of the difficulty of calculating radiative fluxes at the tropopause, which is often ill defined at high latitudes (Wetherald and Manabe 1988). The gain factor for water vapor feedback is slightly positive in the fixed H₂O case because of the shortwave effect of water vapor feedback discussed in section 3. This effect also exists in the control case and is of similar magnitude (0.06). The remainder of the control gain factor is due to the longwave effects of water vapor. The gain factor for cloud feedback is positive in both

models. This is consistent with the results of Wetherald and Manabe (1988), who showed that the cloud feedback related to CO_2 doubling in an atmosphere–mixed layer model whose atmospheric component is very similar to the present model is positive. In fact, the gain factor they calculate is very close to ours (0.11). Although the cloud feedback is slightly stronger in the control model, it is encouraging that the control and fixed H_2O gain factors agree as well as they do. This demonstrates that eliminating water vapor feedback has only a small effect on the magnitude of cloud feedback. The gain factors for albedo feedback are also very similar between the two models, although this is not surprising, since the models have approximately the same mean climate and therefore approximately the same mean sea ice and snow distributions.

In addition to the calculations discussed above, the temperature, water vapor, cloud, and surface albedo changes from the global warming experiments were imposed simultaneously and the global-mean, top-of-the-atmosphere solar and longwave radiative effects of these combined changes were computed using the off-line radiation code. These were then compared to the sum of the radiative effects of the temperature, water vapor, cloud, and surface albedo changes calculated separately. The difference between these two quantities, when divided by the global warming in the two experiments, provided corrections to Λ_c and Λ_f that arise from the radiative interaction of the feedback mechanisms. These corrections were in turn converted to gain factor corrections through division by λ_o . These values are listed in the last row of Table 2. The fact that these corrections are very small relative to the other gain factors is evidence that the feedback mechanisms can be measured separately through their effect on the atmosphere's radiative balance and then combined in a linear fashion without large error.

The radiative interaction of feedback mechanisms is small enough that their associated gain factors may be combined linearly to a fairly good approximation; however, the impacts of feedback mechanisms on the climate's temperature response to an external radiative forcing do not add up linearly, as predicted by Eq. (5). This point may be made more concrete by examining the ratio of the warmings predicted by the gain factors in Table 2. If the gain factors are inserted into Eq. (5), the ratio of the warmings is about 2.8, quite close to the actual ratio of 3.2. However, if the effects of cloud and albedo feedback, both of which are positive feedback mechanisms in this model, are removed from the calculation, the ratio falls to 1.6. Thus the presence of other positive feedback mechanisms enhances the impact of water vapor feedback on the warming. This is why our estimate of the effect of water vapor feedback on global warming is so much larger than previous estimates. This effect may also be seen by examining the geographical dependence of the CO_2 -induced warming in the present models. Figure 7a shows the geographical

distribution of the ratio (control/fixed H_2O) of the local surface warming that occurs by the final century of the global warming experiments. This plot represents the geographical dependence of water vapor feedback's impact on global warming. It is clear from the figure that water vapor feedback has its largest impact at high latitudes. In fact, the ratio of the warmings exceeds 4 over a significant portion of the globe poleward of 50° , especially in the Southern Hemisphere. This is precisely the part of the model world where snow and sea ice are present, especially in the winter. The reason why water vapor feedback has such a strong effect in these regions is because another important positive feedback mechanism, albedo feedback, is present here but not elsewhere.

Although it is not known whether the greenhouse-gas-induced change in cloudiness is a positive or negative feedback to surface temperature in the real climate, we have already noted that cloud feedback is positive in the context of the global warming simulated by both models. This result is consistent with the fact that the ratio of the warmings shown in Fig. 7a is somewhat larger than 2 even over most midlatitude and tropical locations, whereas the ratio predicted by the off-line version when both cloud and albedo feedback are absent was significantly less than 2 (1.6). Thus both cloud and albedo feedback enhance the impact of water vapor feedback in the global warming simulations. Our estimate of water vapor feedback's effect on global warming must therefore be viewed only in the context of the model's other feedback mechanisms. If the albedo or cloud feedbacks had been different in our model, the ratio of the warmings would also have been different.

Other feedback mechanisms affect the apparent impact of water vapor feedback in the unperturbed variability experiments as well. Our estimate of the strength of water vapor feedback in unperturbed variability, based on the control/fixed H_2O ratio of standard deviation of surface temperature, must therefore also be viewed in the context of the model's other feedback mechanisms. For example, the enhancement of water vapor feedback by albedo feedback may be seen by comparing the internally generated local variability of the two models. Figure 7b shows the geographical distribution of the ratio (control/fixed H_2O) of the standard deviation of annual-mean surface temperature. Much of the high latitudes are covered by shaded regions, where the ratio exceeds 1.3. Water vapor feedback has a larger impact on the variability at these locations because albedo feedback comes into play. An analysis of the reason behind the large maximum in the ratio of the variability in the equatorial Pacific is beyond the scope of this paper. However, a model very similar to the control model is known to simulate a phenomenon resembling ENSO (see Knutson et al. 1997). Preliminary analysis, to be presented in a future paper, indicates that fixing water vapor in the radiative transfer subroutine suppresses significantly the model's ENSO-like phenome-

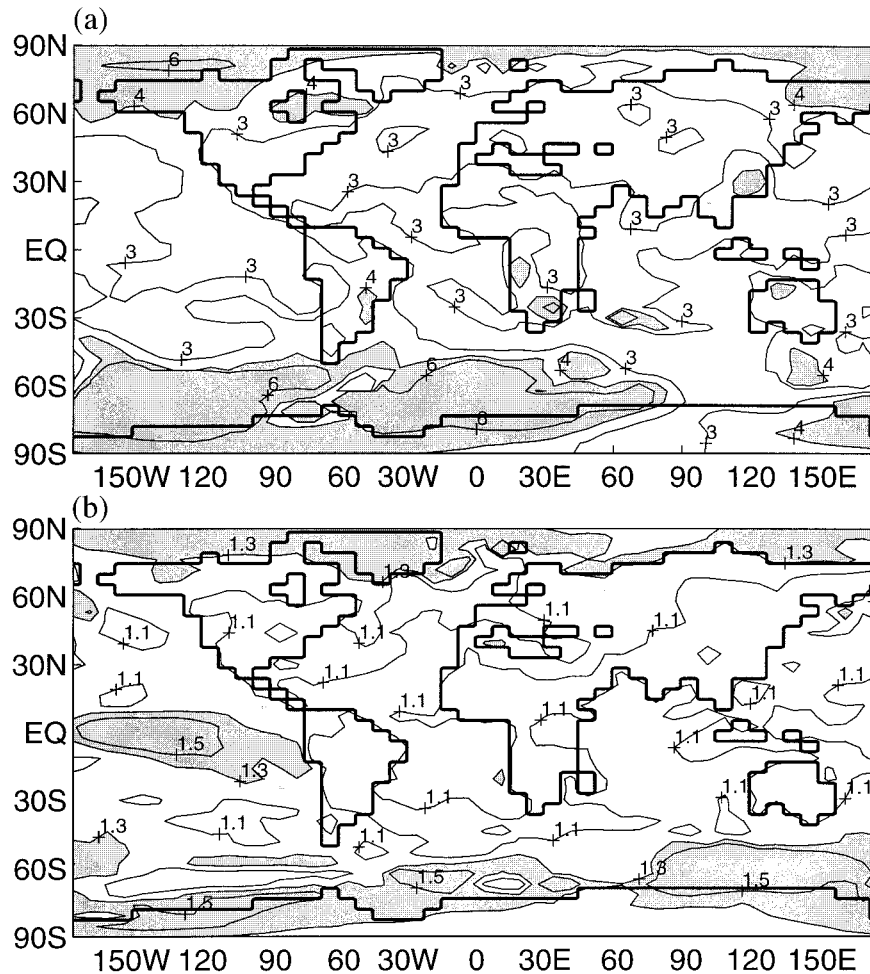


FIG. 7. (a) The geographical distribution of the ratio (control/fixed H₂O) of the local surface warming that took place in the global warming experiments. The ratio was calculated in the following way. First, the average temperature over years 401–500 was calculated at each grid point for both the global warming and unperturbed variability experiments. Then the CO₂ induced warming was calculated at each grid point by taking the difference between these time-averaged values. This procedure was carried out for both control and fixed H₂O cases and a ratio was taken at each grid point. Regions where the ratio exceeds 4 are shaded. In the fixed H₂O global warming experiment, cooling actually occurred in a small region of the circumpolar ocean near 120°W. For the purposes of this contour plot, the ratio of the warming in this region was assumed to be greater than 6. (b) The geographical distribution of the ratio (control/fixed H₂O) of the standard deviation of annual-mean surface temperature. Regions where the ratio exceeds 1.3 are shaded.

non. This drastically reduces surface temperature variability in this region.

In section 5, we compared the impact of water vapor feedback on internally generated anomalies and global warming by comparing the ratio of standard deviation of surface temperature to the ratio of global warming. However, the results of this section make it clear that both of these ratios are affected by other feedback mechanisms. Moreover, the magnitude and sign of the other feedbacks may not be the same in the unperturbed variability and global warming contexts. Thus the ratio of the warmings could be larger than the ratio of the standard deviations because the net strength of the other feedbacks is more positive in the global warming con-

text. Although this is unlikely to account for the large difference in the ratios, it is nevertheless desirable to verify that the difference in the strength of water vapor feedback is mainly responsible for the disparity in the ratios, and that our explanation for the larger impact of water vapor feedback on greenhouse-gas-induced climate change presented in section 5 is therefore robust. A detailed analysis of all feedback mechanisms in the unperturbed variability experiments is a complicated issue that is beyond the scope of this paper. However, it is simple to estimate the radiative strength of water vapor feedback in unperturbed variability using the offline version of the radiative transfer code. Such a calculation facilitates a quantitative comparison of the ra-

diative impact of water vapor feedback in natural variability and global warming contexts isolated from the effects of the other feedbacks. To perform this task, we first regressed annual-mean water vapor time series of the control unperturbed variability experiment at every grid point and vertical level with annual-mean, global-mean surface temperature. These regressions provide a measure of the changes in water vapor that occur throughout the model atmosphere for a global-mean surface temperature anomaly of 1°C . These water vapor anomalies were then imposed on the off-line radiative transfer code and the resulting global-mean decrease in outgoing longwave radiation was calculated. This decrease, when divided by λ_o , gives the gain factor associated with water vapor feedback in natural variability. Using this method, we calculated a gain factor of 0.18 for the longwave effects of water vapor feedback. The global warming counterpart to this gain factor has a value of 0.33 (gain factor listed in Table 2 for water vapor minus the gain factor associated with the shortwave effects of water vapor). This calculation confirms that water vapor feedback is nearly twice as effective in the global warming context, whatever the magnitude and sign of the other feedbacks may be.

7. Conclusions

a. Summary

Here we summarize the picture of water vapor feedback that emerges from our experiments. In section 4, we showed that the control model has more internally generated surface temperature variability on all spatial scales and timescales than its fixed H_2O counterpart. Thus water vapor feedback is positive in the context of the model's unperturbed variability. However, the control/fixed H_2O ratio of standard deviation of surface temperature increases as spatial scales increase. This implies that water vapor feedback is more effective the larger the spatial scale. The degree to which a surface temperature anomaly of a given spatial scale penetrates the troposphere is a critical factor in explaining the spatial-scale dependence of its associated water vapor feedback: global-mean anomalies penetrate more deeply into the troposphere than local ones. Since relative humidity does not change very much as surface temperature fluctuates, this implies a stronger relationship between tropospheric absolute humidity and surface temperature on large scales than small. Water vapor feedback may also become less important at smaller scales because much of the damping of surface-troposphere anomalies is accomplished by horizontal advection of sensible and latent heat, rather than radiative processes, diluting the effects of water vapor feedback.

In section 5, we confirmed that the model's water vapor feedback is also positive in the context of global warming. The equilibrium global warming at the surface due to a doubling of CO_2 in the control experiment was

3.38°C , while for the fixed H_2O case the warming was only 1.05°C . Thus the suppression of internally generated variability by removing a positive feedback also has the effect of reducing the climate sensitivity to an increase in greenhouse gases. However, we also noted that the ratio of equilibrium global warming (control/fixed H_2O) is significantly larger than the ratio of standard deviation of surface temperature in the unperturbed variability experiments at the global spatial scale. Thus the model's water vapor feedback is more effective in global warming than unperturbed variability. Like the explanation for the dependence of water vapor feedback on spatial scale, this difference is rooted in the discrepancy between the tropospheric distribution of the warming in the global warming experiment and the characteristic tropospheric structure of temperature anomalies in the unperturbed variability experiment. In the global warming case, the temperature increase extends throughout the troposphere, whereas in the unperturbed variability case, a typical surface temperature anomaly tends to decrease in amplitude with height. At the same time, simulated surface temperature changes tend to induce very little change in tropospheric relative humidity in both unperturbed variability and global warming cases. For global warming and internally generated temperature anomalies of identical magnitude, there is therefore a smaller change in atmospheric humidity, and hence absorptivity, associated with the internally generated anomaly.

In this section, we also shed light on the reason why internally generated, global-mean temperature anomalies do not penetrate as effectively into the troposphere as the warming induced by a doubling of CO_2 . We showed that when CO_2 increases, the lower-tropospheric warming at a given location is associated with a very similar warming aloft. Thus the global-mean warming is uniform throughout the troposphere as well. Conversely, the regions contributing most to internally generated, global-mean variability in the lower troposphere do not correspond to the regions that contribute most to internally generated, global-mean variability in the mid- to upper troposphere. Temperature fluctuations in the regions that dominate the mid- and upper-tropospheric global-mean variability are most likely only weakly related to temperature fluctuations in the distant regions that dominate the global-mean variability in the lower troposphere. The regression between global-mean tropospheric temperature and surface temperature therefore decreases with height. This points to a difference—of fundamental importance for water vapor feedback—between internally generated, global-mean temperature variability and the global-scale temperature anomaly that results from an increase in CO_2 ; internally generated, global-mean temperature anomalies at any level of the troposphere are a superposition of many modes of variability, whose individual impact is not geographically uniform, and that may not affect all parts of the

troposphere equally. Global warming, on the other hand, is the response to a steady, globally uniform forcing.

Since water vapor feedback has a different impact on internally generated and greenhouse-gas-forced temperature anomalies, it is not straightforward to estimate the climate sensitivity to a doubling of CO_2 based on an analysis of internally generated variability alone. This fact has implications for previous studies. For example, Wigley and Raper (1990) examined low-frequency variability in stochastically forced energy balance models of various sensitivities to assess the probability that the warming trend in global-mean temperature observed over the past 100 yr is internally generated. However, their energy-balance model has the same sensitivity to an increase in greenhouse gases as it does to the low-frequency stochastic forcings they imposed to mimic internally generated, global-mean temperature fluctuations. Our study indicates that this assumption does not apply to the real climate.

The results of sections 4 and 5 are consistent with the original hypothesis that, for the purposes of quantifying the effects of water vapor feedback on surface temperature, water vapor in the model atmosphere is essentially controlled by the Clausius–Clapeyron equation. Whether the context is unperturbed variability or global warming, a surface temperature change is associated with very little change in relative humidity aloft and the atmospheric water vapor content tends to remain proportional to the water vapor storage capacity of the atmosphere. Given this observation, what controls the strength of water vapor feedback is the degree to which a surface temperature anomaly penetrates the troposphere. The more it penetrates, the stronger the water vapor feedback. In the real climate, relative humidity may deviate from constant values to a greater degree than in the model as surface temperature fluctuates (Sun and Held 1996). The vertical structure of a surface–troposphere temperature anomaly is nevertheless a useful starting point from which to gauge the expected strength of its associated water vapor feedback, whether the context is a numerical model or the real climate. This conclusion is consistent with the work of Bony et al. (1995), who analyzed the relationships between tropospheric water vapor, outgoing longwave radiation, and surface temperature in satellite data and output from model experiments in which CO_2 was doubled and the solar constant was increased by 2%. They found that the relationships among these three variables were different depending on whether the type of climate variation under consideration was seasonal and interannual variability, or climate change due to some external forcing. They attributed these differences to the fact that the tropospheric lapse rate behaves differently in the various cases.

In section 6, we examined the interaction between water vapor feedback and other feedback mechanisms. We showed that other feedbacks alter the impact of water vapor feedback. To quantify this effect, we calculated

the radiative impacts of all feedbacks in the CO_2 -induced warming of both models using an off-line version of the model's radiative transfer code. We showed that the surface albedo and cloud feedbacks are positive in both the control and fixed H_2O cases. They therefore act to enhance the apparent impact of water vapor feedback. This interaction among feedback mechanisms explains why our rather large estimate of water vapor feedback's impact on global warming is not in contradiction to previous estimates, which are based on the assumption that water vapor feedback is the only feedback operating and are therefore smaller. Our estimates of the impact of water vapor feedback on unperturbed temperature variability are also affected by the other feedbacks. We therefore verified that it is the difference in water vapor feedback, rather than the other feedbacks, that is the main reason why the control/fixed H_2O ratio of the warming is so much larger than the control/fixed H_2O ratio of unperturbed variability. Using the off-line radiation code, we demonstrated that the changes in water vapor associated with a global mean surface temperature anomaly reduce the radiative damping of surface temperature about half as much as the increase in water vapor associated with a CO_2 -induced global warming anomaly of the same magnitude. This was additional confirmation that water vapor feedback is much stronger in the global warming context. Since the other feedbacks affect the apparent impact of water vapor feedback and may not be perfectly simulated by this model, our estimates of the effect of water vapor feedback should not be taken too literally. Our main conclusions regarding the spatial-scale dependence of water vapor feedback and its differing impact on unperturbed variability and global warming are meant to be robust in a qualitative sense.

b. Discussion: Comparison of observed and modeled variability

In this final section, we place the model's water vapor feedback in the context of the real climate. We assess the realism of the model's water vapor feedback by comparing the surface air temperature variability in the simulations with and without water vapor feedback to the observed surface temperature record. This comparison will allow us to address the following question: Is the model's water vapor feedback necessary to simulate the observed levels of variability?

Figure 8 shows the geographical distribution of standard deviation of annual-mean surface air temperature ($^{\circ}\text{C}$) for three cases: the control unperturbed variability experiment, the observed, and the fixed H_2O unperturbed variability experiment. Although the calculations shown in this figure are based on surface air temperature, rather than surface temperature itself, as elsewhere in this study, the two variables are very tightly linked everywhere on the globe on timescales longer than a few years. For example, analyzing a very similar model,

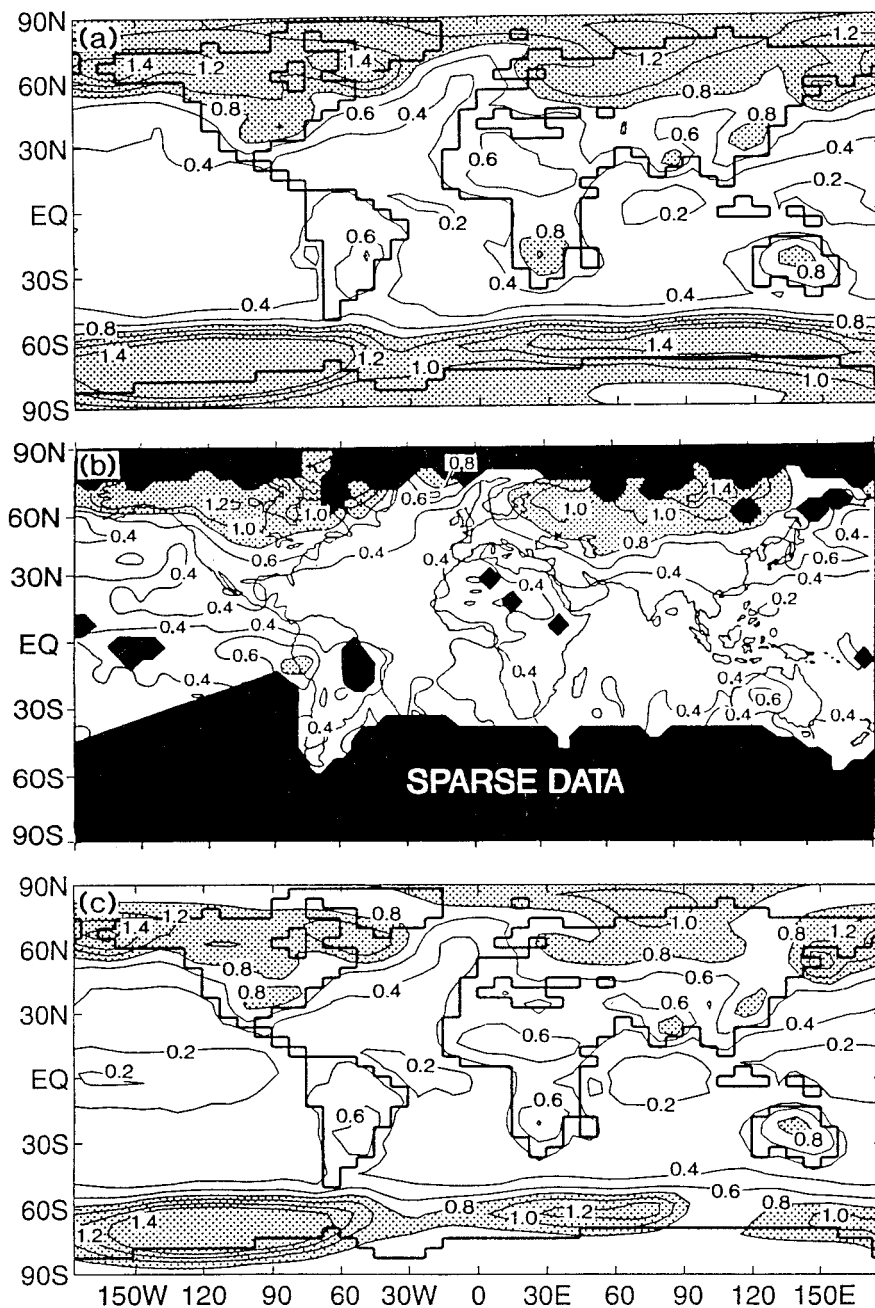


FIG. 8. The geographical distribution of standard deviation of annual-mean surface air temperature ($^{\circ}\text{C}$) for three cases. (a) The control unperturbed variability experiment. (b) The observed standard deviation, as calculated from a 110-yr time series compiled by Jones and Wigley (1991). The standard deviations were calculated by Stouffer et al. (1994), who used the following method. They obtained annual-mean temperature values at those grid points, spaced 5° apart, where at least 10 monthly mean values are available. Standard deviations were then calculated at those grid points where at least 33 annual-mean values are available. (c) The fixed H_2O unperturbed variability experiment.

Manabe and Stouffer (1996) showed that the average spectrum of local sea surface temperature is nearly identical to the average spectrum of local surface air temperature at timescales longer than about two years. The

same would be true at land points at even shorter timescales since the model's land surface has no heat capacity. Thus for the purposes of measuring the low-frequency variability at or near the surface, the two

variables may be used as surrogates for one another. The use of surface air temperature here was dictated by the lack of availability of surface temperature data, particularly over land, where surface air temperature is more commonly measured.

In the mid- to high latitudes of the Northern Hemisphere, both the fixed H₂O and control integrations do a reasonable job of simulating the observed variability. For example, in Fig. 8, the 0.8°C contours of the fixed H₂O and control cases over the North American and Eurasian continents agree equally well with the observed, although they differ somewhat from one another. At the same time, the 0.4°C contours in the North Atlantic agree very well among all three cases. The control experiment shows much more variability in the high latitudes of the Southern Hemisphere than its fixed H₂O counterpart; unfortunately, the observed data necessary to identify the more realistic simulation do not exist in this region. In the Tropics, the standard deviations over land from both experiments agree reasonably well with the corresponding observed standard deviations, so that both models do a respectable job of simulating the observed variability in these regions. In the equatorial Pacific, the standard deviation of surface air temperature in both model configurations is noticeably less than the observed. This is because the model's ENSO-like phenomenon is weaker than observed (Knutson and Manabe 1997). However, this disagreement with observations is much more apparent in the fixed H₂O case, which actually shows a minimum in standard deviation in this region. In addition, the standard deviation in the fixed H₂O case is less than 0.2°C in more areas than either the observed or the control case in the other tropical zones, although the difference is not large.

With the exception of the equatorial Pacific and to a lesser extent the other tropical ocean regions, it cannot be claimed that the control experiment is more realistic than the fixed H₂O; water vapor feedback simply does not have enough impact on local temperature variability to identify one of the two experiments as the more realistic simulation. This leaves open the question of whether water vapor feedback is necessary to reproduce observed levels of variability. However, the picture should be different if global-mean temperature variability is considered. In section 4, we established that water vapor feedback is more effective on larger spatial scales than small. Therefore, an examination of global-rather than local-scale anomalies ought to result in a larger difference between the two unperturbed variability experiments, which will hopefully establish one of the models as the more realistic one. In Fig. 9, we plot the time series of global-mean, annual-mean surface air temperature for four cases. Figure 9a shows the observed time series over the past 110 yr. This time series may be regarded as the observed unperturbed variability, assuming that the warming trend it contains is an internally generated fluctuation of the climate system. Figure 9b shows the same time series with the warming

trend removed. This time series may be regarded as the observed unperturbed variability, assuming that the warming trend of the top panel is entirely due to external forcing. Figures 9c and 9d show the last 400 yr of the control and fixed H₂O time series.

The standard deviations for each time series are shown in their respective panels. With a standard deviation of 0.211°C, the undetrended observed time series exhibits by far the most variability. The large standard deviation is almost entirely due to the warming trend. The detrended observed time series has less variability, with a standard deviation of 0.128°C. The control time series has approximately the same standard deviation as the detrended observed time series (0.127°C), while the fixed H₂O time series has the least variability of all, with a standard deviation of 0.083°C. The relative magnitude of the standard deviations of the two time series from the unperturbed variability experiments is consistent with the results presented in section 4: The presence of water vapor feedback enhances significantly global-scale surface air temperature variability.

We begin the discussion of these results by assuming that the observed warming trend is an internally generated fluctuation and that the topmost panel therefore represents unperturbed variability of surface temperature. Given this assumption, it is clear from both visual inspection of the fixed H₂O and undetrended observed time series and a comparison of their standard deviations that the model without water vapor feedback does not have enough internally generated variability to reproduce the sort of temperature fluctuation seen in the observed undetrended time series. At the same time, the standard deviation of the fixed H₂O time series is also substantially less than that of observed time series with the warming trend removed. Even after minimizing the standard deviation of the observed time series by making the opposite assumption that the warming trend is externally forced, the fixed H₂O model still fails to reproduce the observed unperturbed variability. Therefore, no matter whether we assume the observed trend is internally generated or externally forced, we are unable to simulate the observed global-mean variability without water vapor feedback.

We may make a similar comparison between the observed variability and the control time series. Assuming, again, that the observed warming trend of Fig. 9a is an internally generated fluctuation, the control run also fails to reproduce the observed variability. Not only is the standard deviation of the observed, undetrended time series nearly 70% greater than that of the control case, but nowhere in the control time series is there such a large and sustained trend as is seen in Fig. 9a. This result is consistent with the work of Stouffer et al. (1994), who assessed the probability that a very similar model could reproduce the observed century-scale warming trend without any external forcing. They found that for intervals longer than about 60 yr, no trends as large as the observed trend (0.5°C century⁻¹) can be found in a 1000-yr time series of surface air temperature.

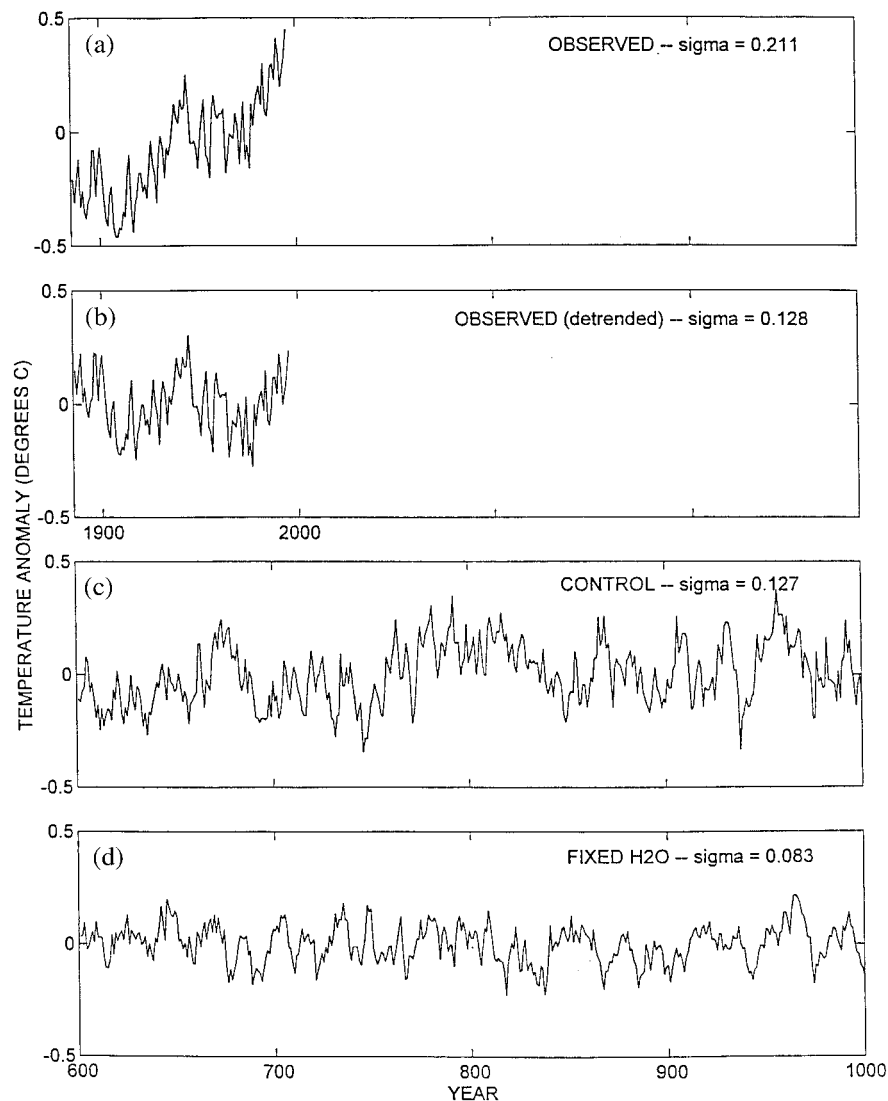


FIG. 9. The time series of global-mean, annual-mean, surface air temperature for four cases. (a) The observed time series over the past 110 yr. (b) The same time series as in (a) with the warming trend removed. The trend was assumed to be linear. (c), (d) The last 400 yr of the control and fixed H_2O time series. The standard deviations for each time series are shown in their respective panels.

Therefore, even with water vapor feedback included, the model still cannot reproduce a fluctuation of the type shown in the topmost panel. The other alternative is to assume the warming is externally forced. In this case, the standard deviations of the control and observed detrended time series agree quite well (although their near-perfect agreement is certainly fortuitous). While a comparison with the observed record reveals definitively that we are unable to simulate the observed levels of variability without water vapor feedback, the model with water vapor feedback has about the right amount of global-scale variability if the observed warming trend is assumed to arise from external forcing.

Acknowledgments. The authors wish to thank Isaac Held, Jerry Mahlman, Brian Soden, and Ron Stouffer for many helpful discussions as well as constructive criticism of the manuscript before it was released for publication. In addition, the article was greatly improved as a result of the comments of two reviewers, Graeme Stephens and Simon Tett. Alex Hall was supported by a NASA Earth System Science Fellowship while this research was being carried out. Observed global-mean surface temperature data were compiled by the Climate Research Unit of the University of East Anglia (United Kingdom) and obtained from their Web site: <http://www.cru.uea.ac.uk:80/cru/data/temperature.htm>.

REFERENCES

- Bony, S., J. P. Duvel, and H. Le Treut, 1995: Observed dependence of the water vapor and clear-sky greenhouse effect on sea surface temperature: Comparison with climate warming experiments. *Climate Dyn.*, **11**, 307–320.
- Bryan, K., 1969: Climate and the ocean circulation: III. The ocean model. *Mon. Wea. Rev.*, **97**, 806–827.
- , and L. Lewis, 1979: A water mass model of the world ocean. *J. Geophys. Res.*, **84** (C5), 2503–2517.
- Cess, R. D., 1989: Gauging water-vapour feedback. *Nature*, **342**, 736–737.
- Dickinson, R. E., V. Meleshko, D. Randall, E. Sarachik, P. Silva-Dias, and A. Slingo, 1996: Climate processes. *Intergovernmental Panel on Climate Change: The Science of Climate Change*, J. T. Houghton et al., Eds., Cambridge University Press, 193–227.
- Gordon, C. T., and W. Stern, 1982: A description of the GFDL Global Spectral Model. *Mon. Wea. Rev.*, **110**, 625–644.
- Haywood, J. M., R. J. Stouffer, R. T. Wetherald, S. Manabe, and V. Ramaswamy, 1997: Transient response of a coupled model to estimated changes in greenhouse gas and sulfate concentrations. *Geophys. Res. Lett.*, **24**, 1335–1338.
- Hering, W. S., and T. R. Borden, 1965: Mean measurements of ozone density over North America, 1963–1964. Environmental Research Papers, Rep. 162, U.S. Air Force Research Laboratory, 27 pp. [Available from AFRL/PA, 1864 4th St., Suite 1, WPAFB, OH 45433-7131.]
- Intergovernmental Panel on Climate Change, 1996: Technical summary. *Climate Change 1995: The Science of Climate Change*, J. T. Houghton et al., Eds., Cambridge University Press, 9–49.
- Jones, P. D., and T. M. L. Wigley, 1991: *Trend '91: A Compendium of Data on Global Change*, T. A. Boden, R. J. Sepanski, and F. W. Stoss, Eds., Oak Ridge National Laboratory, 512–517.
- Kattenberg, A., and Coauthors, 1996: Climate models—Projections of future climate. *Climate Change 1995: The Science of Climate Change*, J. T. Houghton et al., Eds., Cambridge University Press, 285–357.
- Knutson, T. R., S. Manabe, and D. Gu, 1997: Simulated ENSO in a global coupled ocean–atmosphere model: Multidecadal amplitude modulation and CO₂ sensitivity. *J. Climate*, **10**, 138–161.
- Manabe, S., and R. Wetherald, 1967: Thermal equilibrium of the atmosphere with a given distribution of relative humidity. *J. Atmos. Sci.*, **24**, 241–259.
- , and R. J. Stouffer, 1996: Low frequency variability of surface air temperature in a 1000-year integration of a coupled ocean–atmosphere model. *J. Climate*, **9**, 376–393.
- , —, M. Spelman, and K. Bryan, 1991: Transient responses of a coupled ocean–atmosphere model to gradual changes of atmospheric CO₂. Part I: Annual-mean response. *J. Climate*, **4**, 785–817.
- Marotzke, J., and P. Stone, 1995: Atmospheric transports, the thermohaline circulation, and flux adjustments in a simple coupled model. *J. Phys. Oceanogr.*, **25**, 1350–1364.
- Orszag, S. A., 1970: Transform method for calculating vector-coupled sums: Application to the spectral form of the vorticity equation. *J. Atmos. Sci.*, **27**, 890–895.
- Pacanowski, R., K. Dixon, and A. Rosati, 1991: The G.F.D.L Modular Ocean Model users guide. GFDL Ocean Group Tech. Rep. 2, 142 pp. [Available from Geophysical Fluid Dynamics Laboratory/NOAA, P.O. Box 308, Princeton, NJ 08542.]
- Ramanathan, V., and J. A. Coakley, 1978: Climate modeling through radiative-convective models. *Rev. Geophys. Space Phys.*, **16**, 465–489.
- Raval, A., and V. Ramanathan, 1989: Observational determination of the greenhouse effect. *Nature*, **342**, 758–761.
- Redi, M. H., 1982: Oceanic isopycnal mixing by coordinate rotation. *J. Phys. Oceanogr.*, **12**, 1154–1158.
- Stouffer, R. J., S. Manabe, and K. Y. Vinnikov, 1994: Model assessment of the role of natural variability in recent global warming. *Nature*, **367**, 634–636.
- Sun, D. Z., and I. Held, 1996: A comparison of modeled and observed relationships between interannual variations of water vapor and temperature. *J. Climate*, **9**, 665–675.
- Tziperman, E., and K. Bryan, 1993: Estimating global air–sea fluxes from surface properties and from climatological flux data using an oceanic general circulation model. *J. Geophys. Res.*, **98** (C12), 22 629–22 644.
- Wetherald, R. T., and S. Manabe, 1988: Cloud feedback processes in a general circulation model. *J. Atmos. Sci.*, **45**, 1397–1415.
- Wigley, T. M. L., and S. C. B. Raper, 1990: Natural variability of the climate system and detection of the greenhouse effect. *Nature*, **344**, 324–327.